ELSEVIER

Soil Dynamics and Earthquake Engineering 27 (2007) 200–211

SOIL DYNAMICS AND EARTHQUAKE ENGINEERING

www.elsevier.com/locate/soildyn

Stress analysis of buried steel pipelines at strike-slip fault crossings

Dimitrios K. Karamitros, George D. Bouckovalas*, George P. Kouretzis

Department of Geotechnical Engineering, School of Civil Engineering, National Technical University of Athens, 9, Iroon Polytehniou Street, 15780 Athens, Greece

Received 4 April 2006; received in revised form 27 July 2006; accepted 10 August 2006

Abstract

Existing analytical methods for the stress analysis of buried steel pipelines at crossings with active strike-slip faults depend on a number of simplifications, which limit their applicability and may even lead to non-conservative results. The analytical methodology presented herein maintains the well-established assumptions of existing methodologies, but also introduces a number of refinements in order to achieve a more wide range of application without any major simplicity sacrifice. More specifically, it employs equations of equilibrium and compatibility of displacements to derive the axial force applied on the pipeline and adopts a combination of beam-on-elastic-foundation and elastic-beam theory to calculate the developing bending moment. Although indirectly, material and large-displacement non-linearities are also taken into account, while the actual distribution of stresses on the pipeline cross-section is considered for the calculation of the maximum design strain. The proposed methodology is evaluated against the results of a series of benchmark 3D non-linear analyses with the finite element method. It is shown that fairly accurate predictions of pipeline strains may be obtained for a wide range of crossing angles and fault movement magnitudes encountered in practice.

Keywords: Buried steel pipelines; Strike-slip faults; Stress analysis; Design

1. Introduction

Evaluation of the response of buried steel pipelines at active fault crossings is among their top seismic design priorities. This is because the axial and bending strains induced to the pipeline by step-like permanent ground deformation may become fairly large and lead to rupture, either due to tension or due to buckling. Apart from the detrimental effects that such a rupture can have to the operation of critical lifeline systems [1,2], an irrecoverable ecological disaster may also result from the leakage of environmentally hazardous materials such as natural gas, fuel or liquid waste. The currently available techniques of numerical analysis (e.g. large scale Finite Element models) allow a rigorous solution of this problem, minimizing the number of necessary approximations [3]. Nevertheless, the non-linear behavior of the pipeline steel, the soil-pipeline interaction and the second order effects, induced by large displacements, make such analyses rather demanding, and provide ground for the use of simplified analytical methodologies, at least for preliminary design and verification purposes.

A simplified methodology which is widely used today for strike-slip and normal faults, is the one originally proposed by Kennedy et al. [4], and consequently adopted by the ASCE guidelines for the seismic design of pipelines [5]. Kennedy et al. extended the pioneering work of Newmark and Hall [6], by taking into account soil-pipeline interaction in the transverse, as well as in the longitudinal directions. Focusing upon cases where the fault rupture provokes severe elongation of the pipeline, so as tension is the prevailing mode of deformation, Kennedy et al. analyzed the relationship between the axial tensile force, the bending moment and the corresponding axial and bending strains and concluded that:

- the axial tensile force does not depend on the pipeline curvature, as long as bending strains do not exceed 80% of the corresponding axial strains, and that

*Corresponding author. Tel.: +30 2107723870; fax: +30 2108068393.
E-mail address: dimkaram@central.ntua.gr (D.K. Karamitros).

0267-7261/$ - see front matter © 2006 Elsevier Ltd. All rights reserved.
doi:10.1016/j.soildyn.2006.08.001

Nomenclature

a	parameter of the Ramberg–Osgood stress–strain curve
A_s	area of the pipeline cross-section
C	constant, used in Eq. (1b)
C_r	constant of rotational springs on point A and C
D	pipeline diameter
E	Young's modulus of the pipeline steel
E_1	elastic Young's modulus of the pipeline steel
E_2	plastic Young's modulus of the pipeline steel
E_i	initial Young's modulus in the Ramberg–Osgood stress–strain curve
E_{sec}	secant Young's modulus of the pipeline steel
F	axial force
F_a	axial force at the intersection of the pipeline with the fault trace
I	moment of inertia of the pipeline cross section
k	elastic constant of the transverse horizontal soil springs
L	distance from the fault trace
L_{anch}	pipeline unanchored length
L_c	pipeline curved length
M	bending moment
M_{max}	maximum bending moment
q_u	limit stress for transverse soil springs, per pipeline length
r	parameter of the Ramberg–Osgood stress–strain curve
R	radius of curvature
R_m	mean pipeline radius
t	pipeline thickness
t_u	limit soil-pipeline friction force, per pipeline length
V	shear force
w	transverse horizontal displacement of the pipeline
x	position along the pipeline longitudinal axis
β	angle formed by the fault trace and the pipeline axis
δ	transverse displacement of point B
Δf	total fault displacement
ΔL_{av}	available elongation
ΔL_{req}	required elongation
Δx	fault displacement, parallel to the pipeline longitudinal axis
Δy	fault displacement, perpendicular to the pipeline longitudinal axis
ε_1	yield strain of the pipeline steel
ε_a	pipeline axial strain
ε_b	pipeline bending strain
ε_{max}	maximum strain on the pipeline cross-section
ε_{min}	minimum strain on the pipeline cross-section
θ	polar angle of the pipeline cross-section
λ	coefficient defined in Eq. (1c)
σ_1	yield stress of the pipeline steel
σ_y	yield stress in the Ramberg–Osgood stress–strain curve
σ_a	axial stress at the intersection of the pipeline with the fault trace
φ	angle of rotation
φ_1	polar angle defining the part of the cross-section that is under yield due to tension
φ_2	polar angle defining the part of the cross-section that is under yield due to compression

- bending moments become negligible and the pipe behaves essentially as a cable, when the whole pipeline cross-section is under yield.

On these grounds, they consequently ignored the pipeline bending stiffness, claiming that even when the above criteria are not met, their analysis would overestimate the pipeline curvature and the associated bending strains.

It becomes evident that the Kennedy et al. criteria are met only when the pipeline is subjected to large fault movements and is able to undergo large tensile strains without rupture. However, in practice, special construction measures (e.g. stringent welding procedures, special inspection and confirmation through laboratory tests) are required in order to satisfy this condition. In common cases, where such measures have not been approved, the maximum allowable strain is seriously reduced compared to that of the pipeline steel, in order to account for thermal effects and metallurgical alterations induced by welding. For such strain levels (e.g. 0.5%), which are well out of the range specified by the Kennedy et al. criteria, analytically predicted strains may become even one order of magnitude larger than the actual ones.

Wang and Yeh [7] tried to overcome this shortcoming by taking the pipeline bending stiffness into account. Their methodology refers only to strike-slip faults and relies on partitioning of the pipeline into four (4) distinct segments (Fig. 1): two (2) in the high curvature zone on both sides of the fault trace, and another two (2) outside this zone. The latter segments are treated as beams-on-elastic-foundation, while the former ones are assumed to deform as circular arcs, with a radius of curvature calculated from the equations of equilibrium and the demand for continuity between adjacent segments. In this way, the bending moment at the conjunction of each arc with its neighboring elastic beam can be readily calculated and consequently compared to the pipeline's ultimate moment capacity, in order to estimate a factor of safety against failure. In addition, a second factor of safety is calculated at the point of intersection with the fault trace, as the ratio of the pipeline ultimate strain over the corresponding axial strain.

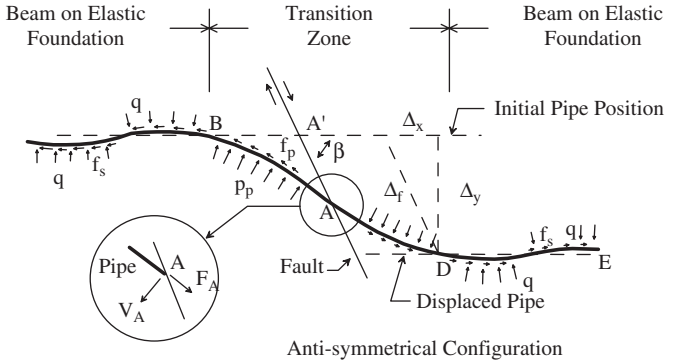

Fig. 1. Pipeline analysis model proposed by Wang and Yeh [7].

Although clearly advanced, compared to the methodology of Kennedy et al. [4], the methodology of Wang and Yeh also features some pitfalls. Namely:

- The axial force is merely taken into account for reducing the pipeline's ultimate moment capacity, while its unfavorable contribution to bending stiffness is overlooked.
- The most unfavorable combination of axial and bending strains does not necessarily develop at the end of the high-curvature zone (points B and D in Fig. 1) as the method assumes, but within this zone, closer to the intersection with the fault trace (point A in Fig. 1).
- The calculation of a safety factor in terms of bending moments may be misleading for displacement-controlled problems, such as the one at hand, where strain or deformation acceptance criteria are more appropriate [3].

Based on the well established concepts inherited by existing methodologies, such as the equations used by Kennedy et al. [4] to quantify the effect of axial tension on the pipeline curvature and the partitioning of the pipeline into four (4) segments first introduced by Wang and Yeh [7], the proposed methodology attempts to eliminate the abovementioned setbacks by introducing a number of critical refinements. Its validity and its range of application are evaluated through comparison with typical analytical predictions obtained with the methodologies of Kennedy et al. [4] and Wang and Yeh [7], as well as with more accurate numerical predictions, based on the 3D non-linear Finite Element Method.

2. Methodology outline

In more detail, the proposed methodology computes axial and bending strains along the pipeline with the aid of beam-on-elastic-foundation and elastic-beam theories, taking into account the bending stiffness of the pipeline cross-section, as well as the soil-pipeline interaction effects in both the axial and the transverse directions. Material non-linearity is considered by assuming a bilinear stress–strain relationship for the pipeline steel, combined with an iterative linear elastic solution scheme which uses the secant Young's modulus of the pipeline steel in order to ensure compatibility between computed non-linear stresses and strains.

The strike-slip fault is taken as an inclined plane, i.e. with null thickness of rupture zone, so that the intersection of the pipeline axis with the fault trace on the ground surface is reduced to a single point. The fault movement is defined in a Cartesian coordinate system, where the x-axis is collinear with the undeformed longitudinal axis of the pipeline, while the y-axis is perpendicular to x in the horizontal plane (Fig. 2). Subsequently, the fault movement is analyzed into two Cartesian components, Δx and Δy, interrelated through the angle formed by the x-axis and the fault trace (angle β in Fig. 2). In its present form, the proposed method applies to crossing angles $\beta \leqslant 90^\circ$, resulting in pipeline elongation.

Following the general concept originally introduced by Wang and Yeh [7], the pipeline is partitioned into four (4) segments, defined by the characteristic points A, B and C in Fig. 3: Point B is the intersection of the pipeline axis with the fault trace, while points A and C are the closest points of the pipeline axis with zero y displacement. Then, the computation of combined axial and bending pipeline strains proceeds in six (6) steps:

1. Segments AA′ and CC′ are analyzed as beams-on-elastic-foundation in order to obtain the relation between shear force, bending moment and rotation angle at points A and C.
2. Considering the boundary conditions determined in step 1, segments AB and BC are analyzed according to the elastic-beam theory in order to derive the maximum bending moment.
3. The axial force on the pipeline, at the intersection with the fault trace (point B), is obtained by equalizing the required and the available pipeline elongation.
4. Bending strains are calculated, accounting for geometric second-order effects.
5. The maximum pipeline strain is computed from the demand for equilibrium between the externally applied axial force and the internal stresses developing on the pipeline cross-section.

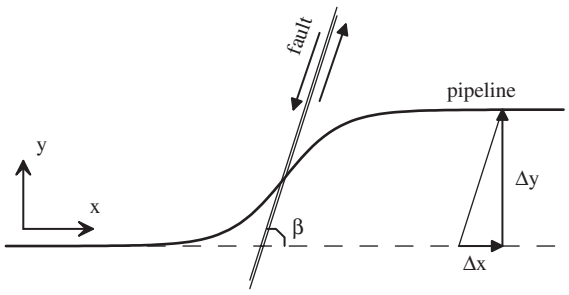

Fig. 2. Definition of axes x and y and fault displacements Δx and Δy.

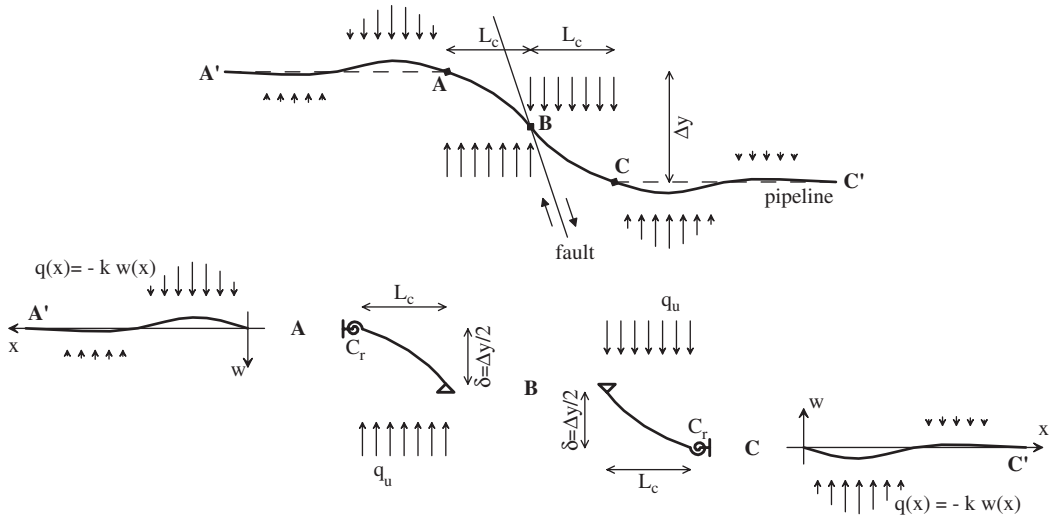

Fig. 3. Partitioning of the pipeline into four segments.

6. Finally, given the stress and strain distribution within the cross-section, an updated secant Young's modulus is computed and steps 2–6 are repeated until convergence is accomplished.

As in all similar design methodologies [4,6,7], the above solution algorithm overlooks initial pipeline stresses due to soil overburden, as they are fairly small compared to the ones developing due to fault movement. Furthermore, pipeline and soil inertia effects are not taken into account as the velocity of the sliding part of the fault is considered to be sufficiently small, while concurrent spatially variable transient motion is neglected in the computations. Finally, it should be stressed that the proposed methodology overlooks local buckling and section deformation effects [8], two phenomena which dominate pipeline behavior at large fault displacements. As a result, its application range is limited within the allowable strains which are explicitely defined by design codes [3,9] in order to avoid such detrimental effects. For larger strain levels, rigorous numerical methods, or large displacement approximate methods [10] should be used.

3. Solution algorithm

3.1. Step 1

The differential equilibrium equation for the elastic line of segment AA′ (Fig. 3) is:

$$E_1 I w'''' + kw = 0. \tag{1a}$$

Imposing $w = 0$ for $x = 0$ and $w \to 0$ for $x \to \infty$, Eq. (1) yields:

$$w = Ce^{-\lambda x} \sin \lambda x, \tag{1b}$$

where

$$\lambda = \sqrt[4]{\frac{k}{4E_1 I}}, \tag{1c}$$

where x is the distance from point A along the pipeline axis, w is the transverse horizontal displacement, E_1 is the elastic Young's modulus of the pipeline steel, I is the moment of inertia of the pipeline cross-section, and k is the constant of the transverse horizontal soil springs (Fig. 4a). According to the ALA-ASCE [3] guidelines, computation of k can be based on Hansen [11] and Trautmann and O'Rourke [12].

Differentiation of Eq. (1a) yields the following relations between the shear force $V_A = -E_1 I w'''_A$, the bending moment $M_A = -E_1 I w''_A$ and the rotation $\phi_A = w'_A$ at point A:

$$M_A = (2\lambda E_1 I)\phi_A, \tag{2}$$

$$V_A = -\lambda M_A. \tag{3}$$

Due to symmetry, similar relations apply for point C.

3.2. Step 2

Due to symmetry, the analysis can be focused on segment AB. This segment is modeled as an elastic beam, supported at point A by a rotational spring, whose constant is calculated from Eq. (2) as $C_r = 2\lambda E_1 I$, and at point B by a joint, which is displaced by half the transverse component of the strike-slip fault movement, i.e. $\delta = \Delta y/2$. As a result, a uniformly distributed load q_u is applied to the beam, equal to the limit value of soil reaction for transverse horizontal movement of the pipeline relatively to the surrounding soil (Fig. 4b). According to the ALA–ASCE [3] guidelines, the value of q_u can be calculated from the properties of the backfill of the pipeline trench, based on the relations proposed by Hansen [11] and Trautmann and O'Rourke [12].

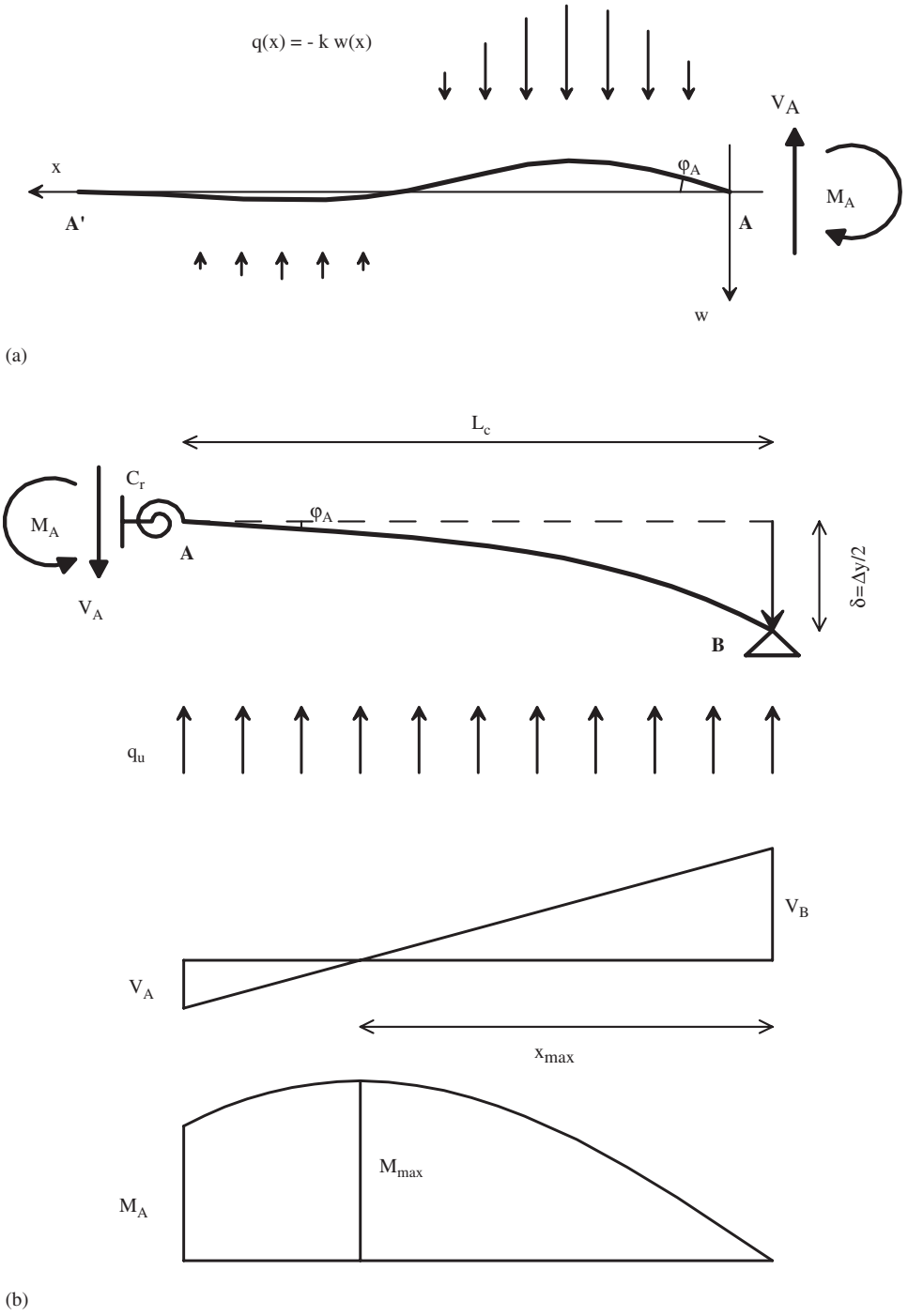

Fig. 4. Analysis model for pipeline segments 1 (a) and 2 (b).

Application of the elastic-beam theory yields the following bending moment and shear force reactions on the supports A and B:

$$M_{\mathrm{A}} = \frac{24EI\delta C_{\mathrm{r}} - q_{\mathrm{u}} C_{\mathrm{r}} L_{\mathrm{c}}^4}{24EIL_{\mathrm{c}} + 8C_{\mathrm{r}} L_{\mathrm{c}}^2}, \tag{4}$$

$$V_{\mathrm{A}} = \frac{24EI\delta C_{\mathrm{r}} - 12EIq_{\mathrm{u}} L_{\mathrm{c}}^3 - 5q_{\mathrm{u}} C_{\mathrm{r}} L_{\mathrm{c}}^4}{24EIL_{\mathrm{c}}^2 + 8C_{\mathrm{r}} L_{\mathrm{c}}^3}, \tag{5}$$

$$V_{\mathrm{B}} = \frac{24EI\delta C_{\mathrm{r}} + 12EIq_{\mathrm{u}} L_{\mathrm{c}}^3 + 3q_{\mathrm{u}} C_{\mathrm{r}} L_{\mathrm{c}}^4}{24EIL_{\mathrm{c}}^2 + 8C_{\mathrm{r}} L_{\mathrm{c}}^3}. \tag{6}$$

Eqs. (4)–(6) express the reaction forces of segments AB and BC in terms of the curved length L_{c} of the beam, which is not a priori known. However, substituting Eqs. (4) and (5) into Eq. (3) yields:

$$a_5 L_{\mathrm{c}}^5 + a_4 L_{\mathrm{c}}^4 + a_3 L_{\mathrm{c}}^3 - a_1 L_{\mathrm{c}} - a_0 = 0, \tag{7a}$$

where a_0–a_5 are known constants, equal to:

$$a_0 = 24EI\delta C_r,$$
$$a_1 = 24EI\delta C_r\lambda,$$
$$a_3 = 12EIq_u,$$
$$a_4 = 5q_uC_r,$$
$$a_5 = q_uC_r\lambda. \quad (7b)$$

The above polynomial equation can be solved iteratively, using the Newton–Raphson method, with a large initial value for L_c (e.g. 500 m). In this way, the values of M_A, V_A, and V_B can be directly estimated, and the maximum bending moment developing on the pipeline can be consequently calculated from the elastic-beam theory, as:

$$M_{max} = V_B x_{max} - \frac{q_u x_{max}^2}{2}, \quad (8a)$$

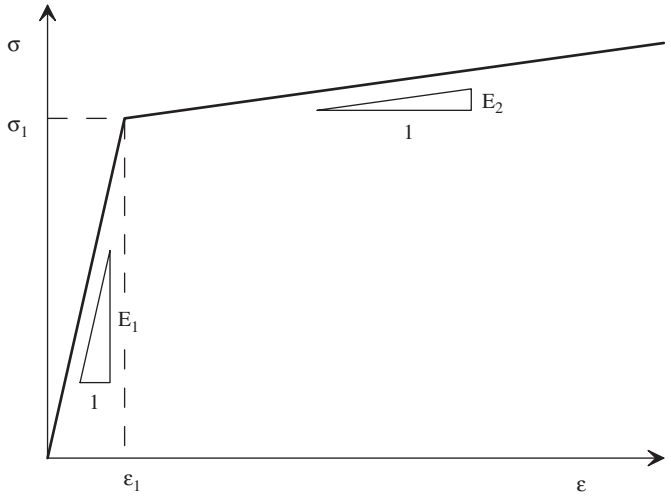

Fig. 5. Assumed bilinear stress-strain relationship for the pipeline steel.

where

$$x_{max} = \frac{V_B}{q_u}. \quad (8b)$$

3.3. Step 3

Similar to all existing methodologies [4,6,7], the axial force at the intersection of the pipeline with the fault trace is calculated from the requirement for compatibility between the geometrically required and the stress-induced (available) pipeline elongation. The required elongation ΔL_{req} is defined as the elongation imposed to the pipeline due to the fault movement. For the sake of simplicity, the elongation provoked by the Δy fault displacement component may be neglected, as it is minimal compared to the elongation due to the Δx component. Therefore:

$$\Delta L_{req} \approx \Delta x. \quad (9)$$

On the other hand, the available elongation ΔL_{av} is defined as the elongation resulting from the integration of axial strains along the unanchored length, i.e. the length over which slippage occurs between the pipeline and the surrounding soil:

$$\Delta L_{av} = 2\int_0^{L_{anch}} \varepsilon(L)\,dL, \quad (10)$$

where L is the distance from the fault trace, while the factor 2, by which the integral in Eq. (10) is multiplied, accounts for the elongation on both sides of the fault trace.

The unanchored length L_{anch} may be calculated from the equilibrium along the pipeline axis, assuming that axial pipeline stresses essentially become zero at the far end of the unanchored length. In this way, L_{anch} is expressed as:

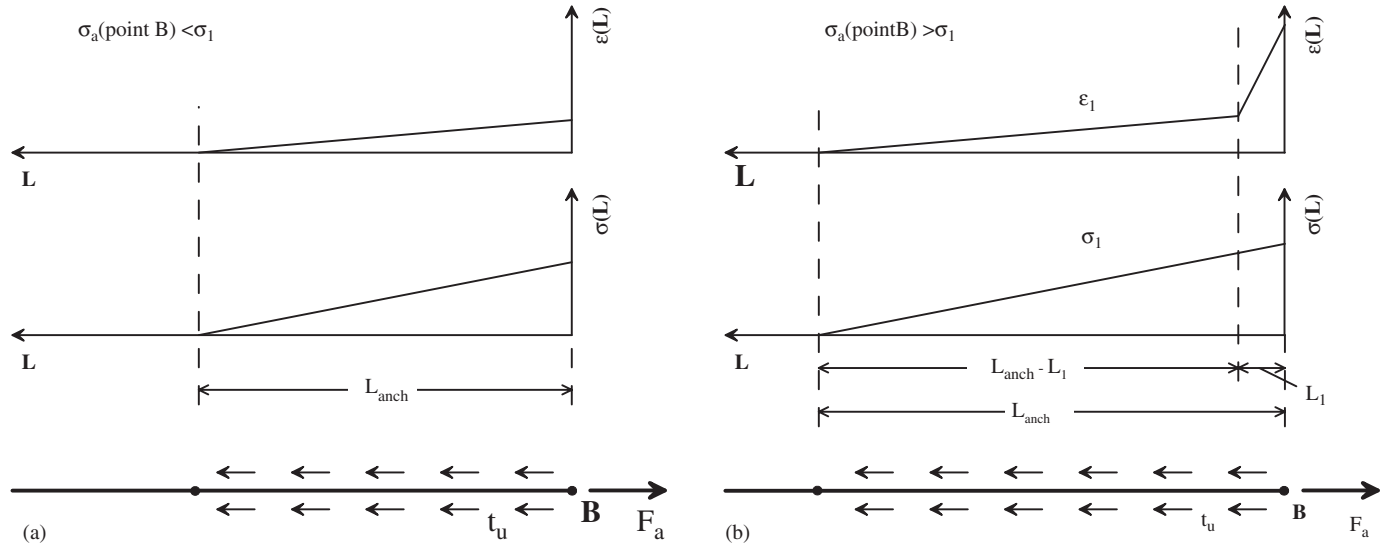

Fig. 6. Linear (a) and non-linear (b) stress and strain variation along the pipeline's unanchored length.

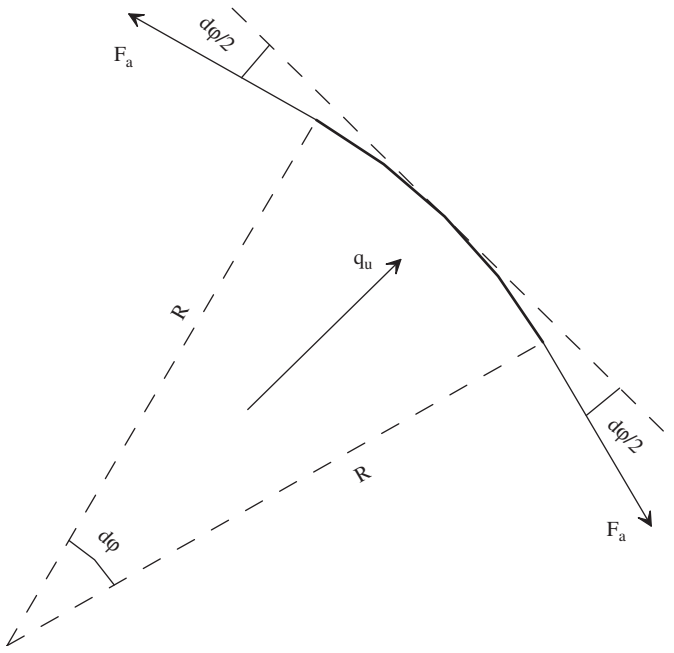

Fig. 7. Effect of the applied axial force on the pipeline curvature.

$$L_{\text{anch}} = \frac{F_a}{t_u} = \frac{\sigma_a A_s}{t_u}, \tag{11}$$

where F_a and σ_a are the axial force and stress developing in the intersection of the pipeline axis with the fault trace, A_s is the area of the pipeline cross-section and t_u is the limit friction due to the slippage of the pipeline relatively to the surrounding soil [3].

The distribution of strains along the unanchored length can be consequently derived from the corresponding stresses, assuming a bilinear stress–strain relationship for the pipeline steel (Fig. 5). Assuming further that axial stresses attenuate linearly with the distance from the fault trace, due to the constant value of the limit friction force, tensile stresses along the pipeline axis can be expressed as:

$$\sigma(L) = \sigma_a - \frac{t_u}{A_s} L. \tag{12}$$

For the case where the axial tensile stress σ_a is below the yield limit σ_1 (Fig. 6a), Eq. (10) can be re-written as:

$$\Delta L_{av} = 2\int_0^{L_{\text{anch}}} \frac{\sigma(L)}{E_1}\,dL = \frac{\sigma_a^2 A_s}{E_1 t_u}. \tag{13}$$

Therefore, for $\Delta L_{av} = \Delta L_{req}$, the maximum tensile stress becomes:

$$\sigma_a = \sqrt{\frac{E_1 t_u \Delta L_{req}}{A_s}}. \tag{14}$$

If the required elongation is larger than the one corresponding to $\sigma_a = \sigma_1$, i.e. when:

$$\Delta L_{req} > \frac{\sigma_1^2 A_s}{E_1 t_u} \tag{15}$$

then plastic strains develop in the pipeline (Fig. 6b) and Eq. (10) becomes:

$$\Delta L_{av} = 2\left[\int_0^{L_1}\left(\varepsilon_1 + \frac{\sigma(L)-\sigma_1}{E_2}\right)dL + \int_{L_1}^{\text{Lanch}} \frac{\sigma(L)}{E_1}\,dL\right], \tag{16}$$

where

$$L_1 = \frac{(\sigma_a - \sigma_1)A_s}{t_u}. \tag{17}$$

Combining Eq. (11), (12), (16) and (17), the maximum developing tensile stress becomes:

$$\sigma_a = \frac{\sigma_1(E_1 - E_2) + \sqrt{\sigma_1^2(E_2^2 - E_1E_2) + E_1^2 E_2 \Delta L_{req}\frac{t_u}{A_s}}}{E_1}. \tag{18}$$

Regardless of the axial stress level, the corresponding axial force is equal to:

$$F_a = \sigma_a A_s. \tag{19}$$

3.4. Step 4

According to the elastic beam theory, bending strains on the pipeline can be calculated as:

$$\varepsilon_b^{\text{I}} = \frac{M_{\max} D}{2EI}, \tag{20}$$

where D is the external pipeline diameter.

The above equation is accurate for small fault displacements, while for larger fault displacements, geometrical second-order effects must be also taken into account. To simplify this relatively complex problem, the bending stiffness of the pipeline may be approximately neglected [4], so that bending strains can be computed geometrically as:

$$\varepsilon_b^{\text{II}} = \frac{D/2}{R}. \tag{21}$$

The radius of curvature R results from the equilibrium of the forces acting on an infinitesimal part of the pipeline's curved length (Fig. 7):

$$R = \frac{F_a}{q_u} \tag{22}$$

and finally:

$$\varepsilon_b^{\text{II}} = \frac{q_u D}{2F_a}. \tag{23}$$

Eq. (23) indicates that bending strains induced by second-order effects are inversely proportional to the axial force applied on the pipeline. In other words, for small fault displacements, bending strains computed by Eq. (23) tend to become infinite. This is due to the fact that Eq. (22) has been derived assuming that the pipeline bending

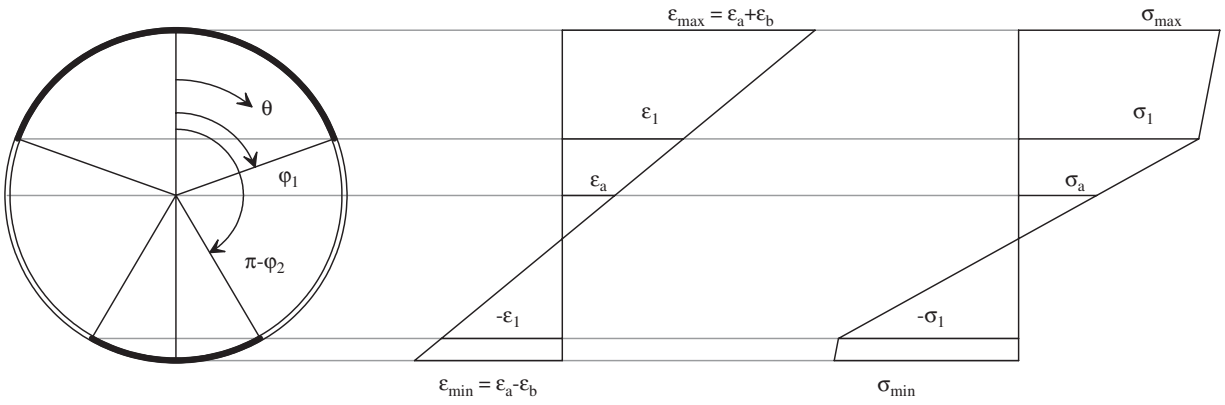

Fig. 8. Non-linear stress and strain distribution on the pipeline cross-section.

stiffness is equal to zero, which is approximately true only when the whole pipeline cross-section is under yield.

According to the above, the actual bending strain ε_b lays between ε_b^I and ε_b^{II}, asymptotically approaching ε_b^I as fault displacements tend to zero and ε_b^{II} in the opposite case. Here, it is approximately assumed that:

$$\frac{1}{\varepsilon_b} = \frac{1}{\varepsilon_b^I} + \frac{1}{\varepsilon_b^{II}}. \tag{24}$$

3.5. Step 5

Existing methodologies [4,6,7] calculate the axial strain directly from the axial stress, using the adopted stress–strain relation for the pipeline steel. When strains in the pipeline cross-section remain in the elastic range, this assumption is valid for every point along the pipeline axis. However, when yielding occurs, it is accurate only at the intersection of the pipeline with the fault trace, where the bending strain is zero. In the vicinity of the cross-section where the maximum bending strain occurs, axial strain increases locally, so that the integral of stresses on the pipeline cross-section remains equal to the applied axial force.

This effect of curvature on the relation between the applied axial force and the corresponding axial strain was in fact acknowledged by Kennedy et al. [4], but the Ramberg–Osgood stress–strain curve, which they adopted to approximate steel behavior, inhibited the derivation of a simple relation to quantify this effect. Therefore, Kennedy et al. were limited to performing a numerical investigation of the strain range for which this interaction could be ignored.

In the present work, the interaction between axial and bending strains is quantified by determining the exact distribution of strains and stresses on the pipeline cross-section. For this purpose, the beam-theory assumption of plane cross-sections is embraced, while the stress–strain curve of the pipeline steel is considered to be bilinear (Fig. 5).

Bearing in mind the above, the strain distribution on the cross-section is given by Eq. (25):

$$\varepsilon = \varepsilon_a + \varepsilon_b \cos\theta, \tag{25}$$

where the angle θ is the polar angle of the cross-section, defined in Fig. 8. The corresponding distribution of stresses on the pipeline cross-section is given by Eq. (26):

$$\sigma = \begin{cases} \sigma_1 + E_2(\varepsilon - \varepsilon_1), & 0 \leqslant \theta < \phi_1, \\ E_1\varepsilon, & \phi_1 \leqslant \theta \leqslant \pi - \phi_2, \\ -\sigma_1 + E_2(\varepsilon + \varepsilon_1), & \pi - \phi_2 < \theta \leqslant \pi, \end{cases} \tag{26}$$

where the angles $\varphi_{1,2}$ define the portion of the cross-section that is under yield (Fig. 8), and are calculated as:

$$\phi_{1,2} = \begin{cases} \pi, & \dfrac{\varepsilon_1 \mp \varepsilon_a}{\varepsilon_b} < -1, \\ \arccos\left(\dfrac{\varepsilon_1 \mp \varepsilon_a}{\varepsilon_b}\right), & -1 \leqslant \dfrac{\varepsilon_1 \mp \varepsilon_a}{\varepsilon_b} \leqslant 1, \\ 0, & 1 < \dfrac{\varepsilon_1 \mp \varepsilon_a}{\varepsilon_b}. \end{cases} \tag{27}$$

The total axial force is calculated by integrating the stresses over the cross-section, as:

$$\begin{aligned} F &= 2\int_0^{\pi} \sigma R_m t \, d\theta \\ \Rightarrow F &= 2R_m t\big[E_1\pi\varepsilon_a - (E_1 - E_2)(\phi_1 + \phi_2)\varepsilon_a \\ &\quad + (E_1 - E_2)(\phi_1 - \phi_2)\varepsilon_1 \\ &\quad - (E_1 - E_2)(\sin\phi_1 - \sin\phi_2)\varepsilon_b\big], \end{aligned} \tag{28}$$

where

$$R_m = \frac{D - t}{2}. \tag{29}$$

The axial strain of the pipeline can be derived from the demand for equilibrium, by equating the axial force computed using Eq. (28), to the one calculated using Eq. (19). Note that Eq. (19) applies strictly at the pipeline's intersection with the fault trace, but it is approximately extended to the neighboring position of the maximum bending moment. The solution of the system of Eqs. (27) and (28) results in a complex formula for ε_a, which can be

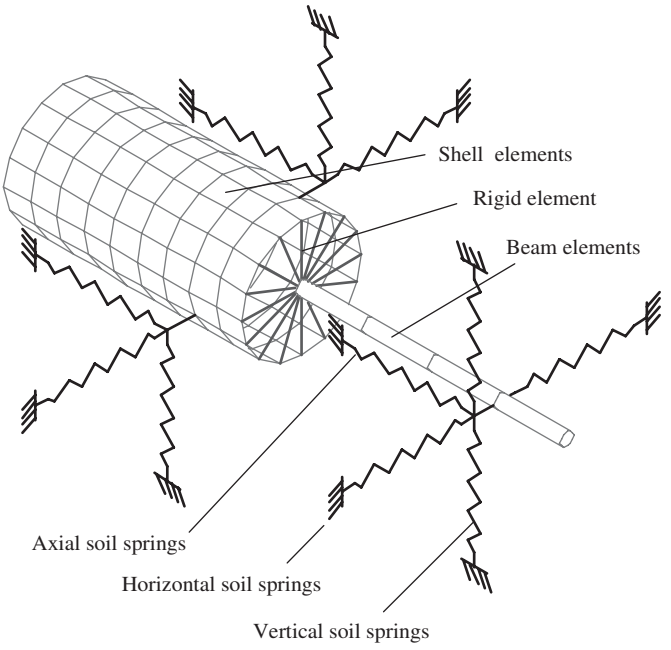

Fig. 9. 3D model used for analyses with the Finite Element Method: the junction between shell and beam part.

solved iteratively, using the Newton–Raphson method. Namely, using an initial value of $\varepsilon_a^0 = 0$, the axial strain on each iteration can be calculated as:

$$\varepsilon_a^{k+1} = \varepsilon_a^k - \frac{F(\varepsilon_a^k) - F_a}{\mathrm{d}F/\mathrm{d}\varepsilon_a\big|_{\varepsilon_a=\varepsilon_a^k}}, \tag{30}$$

where

$$\frac{\mathrm{d}F}{\mathrm{d}\varepsilon_a} = 2R_m t\Bigg[E_1\pi - (E_1-E_2)(\phi_1+\phi_2) - (E_1-E_2) \times\left(\frac{\mathrm{d}\phi_1}{\mathrm{d}\varepsilon_a}+\frac{\mathrm{d}\phi_2}{\mathrm{d}\varepsilon_a}\right)\varepsilon_a + (E_1-E_2)\left(\frac{\mathrm{d}\phi_1}{\mathrm{d}\varepsilon_a}-\frac{\mathrm{d}\phi_2}{\mathrm{d}\varepsilon_a}\right)\varepsilon_1 -(E_1-E_2)\left(\frac{\mathrm{d}\phi_1}{\mathrm{d}\varepsilon_a}\cos\phi_1-\frac{\mathrm{d}\phi_2}{\mathrm{d}\varepsilon_a}\cos\phi_2\right)\varepsilon_b\Bigg] \tag{31}$$

and

$$\frac{\mathrm{d}\phi_{1,2}}{\mathrm{d}\varepsilon_a} = \begin{cases} \pm\dfrac{1}{\varepsilon_b\sin\phi_{1,2}}, & \varepsilon_b\sin\phi_{1,2} \leqslant -0.01, \\ -100, & -0.01 < \varepsilon_b\sin\phi_{1,2} \leqslant 0, \\ \pm 100, & 0 < \varepsilon_b\sin\phi_{1,2} \leqslant 0.01, \\ \pm\dfrac{1}{\varepsilon_b\sin\phi_{1,2}}, & 0.01 < \varepsilon_b\sin\phi_{1,2}. \end{cases} \tag{32}$$

The limits of $\mathrm{d}\phi_{1,2}/\mathrm{d}\varepsilon_a$ proposed in Eq. (32) are more or less arbitrary, but significantly accelerate the iterative process.

Having calculated the axial strain at the position of maximum bending strain, the minimum and maximum longitudinal strains can be subsequently computed as their algebraic sum (i.e. $\varepsilon_{max,min} = \varepsilon_a \pm \varepsilon_b$).

Table 1
API5L-X65 steel properties considered in the numerical analyses

Yield stress (σ_1)	490 MPa
Failure stress (σ_2)	531 MPa
Failure strain (ε_2)	4.0%
Elastic Young's modulus (E_1)	210 GPa
Yield strain ($\varepsilon_1 = \sigma_1/E_1$)	0.233%
Plastic Young's modulus ($E_2 = (\sigma_2 - \sigma_1)/(\varepsilon_2 - \varepsilon_1)$)	1.088 GPa

Table 2
Parameters of the Ramberg–Osgood stress–strain curve for steel type API5L-X65

Initial Young's modulus (E_1)	210 GPa
Yield stress (σ_y)	490 MPa
a	38.32
r	31.50

Table 3
Soil spring properties considered in the numerical analyses

	Yield force (kN/m)	Yield displacement (mm)
Axial (friction) springs	40.5	3.0
Transverse horizontal springs	318.6	11.4
Vertical springs (upward movement)	52.0	2.2
Vertical springs (downward movement)	1360.0	100.0

3.6. Step 6

The analysis of segments AB and BC, from which the maximum bending moment emerges, is based on the elastic beam theory and is not taking into account the non-linear behavior of the pipeline steel. Since the steel stress–strain relationship is considered to be bilinear (Fig. 5), a series of equivalent linear calculation loops is performed, employing a procedure for readjusting the secant Young's modulus of the pipeline steel on each loop.

More specifically, using the already defined stress distribution on the pipeline cross-section, the corresponding bending moment can be calculated using Eq. (33):

$$M = 2\int_0^{\pi}\sigma R_m t R_m\cos\theta\,\mathrm{d}\theta$$

$$\Rightarrow M = 2R_m^2 t\Bigg[\frac{E_1\pi\varepsilon_b}{2} - (E_1-E_2)(\sin\phi_1-\sin\phi_2)\varepsilon_a + (E_1-E_2)(\sin\phi_1+\sin\phi_2)\varepsilon_1 - \frac{(E_1-E_2)(\phi_1+\phi_2)\varepsilon_b}{2} - \frac{(E_1-E_2)(\sin 2\phi_1+\sin 2\phi_2)\varepsilon_b}{4}\Bigg]. \tag{33}$$

Therefore, the secant modulus for the next iteration can be calculated as:

$$E'_{sec} = \frac{M(\varepsilon_a,\varepsilon_b)D}{2I\varepsilon_b^{I}} = \frac{M(\varepsilon_a,\varepsilon_b)D}{2I}\left(\frac{1}{\varepsilon_b}-\frac{1}{\varepsilon_b^{II}}\right) \tag{34}$$

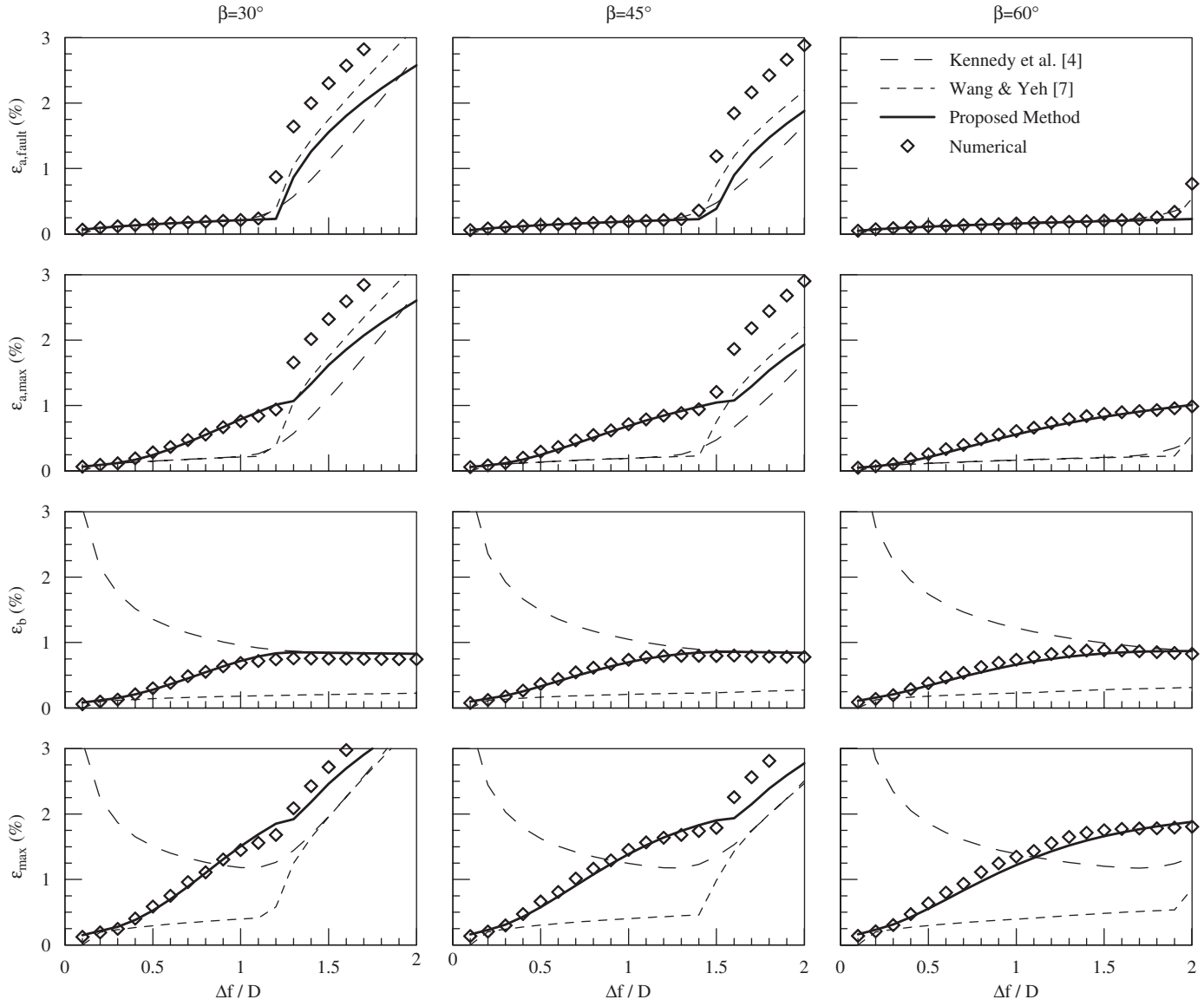

Fig. 10. Comparison of the results of the proposed analytical methodology with the results of the numerical analyses and the predictions of the Kennedy et al. [4] and Wang and Yeh [7] methods.

and steps 2–6 are repeated, until convergence is accomplished.

4. Validation of the proposed methodology

To validate the results of the proposed methodology, analytical predictions are compared to the results from a series of 3D non-linear numerical analyses with the Finite Element Method, performed with the commercial code MSC/NASTRAN [13]. For this purpose, a typical high-pressure natural gas pipeline was considered, featuring an external diameter of 0.9144 m (36 in), a wall thickness of 0.0119 m (0.469 in), and a total length of 1000 m.

A hybrid model was used for the simulation of the pipeline, with a part of 50 m along both sides of the fault trace (i.e. a total length of 100 m) modeled as a cylindrical shell, and the remaining 450 m part (i.e. a total length of 900 m) modeled as a beam (Fig. 9). The shell perimeter was discretized into 16 equal sized quadrilateral shell elements, each of 0.20 m length. CQUAD4 type elements were used, namely isoparametric quadrilateral shell elements, with both bending and membrane stiffness [13]. The beam part was discretized with 0.50 m long CBEAM type beam elements, with extension, bending and shearing stiffness [13].

To simulate soil-pipeline interaction effects, each node of the model was connected to axial, transverse horizontal and vertical soil springs, modeled as elastic-perfectly plastic CROD type rod elements [13]. Thus, the Finite Element Model used herein consisted of a total number of 32,252

nodes and 32,236 elements and had 58,710 degrees of freedom.

The pipeline steel was of the API5L-X65 type, with a bilinear elasto-plastic stress–strain curve (Fig. 5) and the properties listed in Table 1. Note that the numerical analyses were also performed using an equivalent Ramberg–Osgood stress–strain curve, i.e.:

$$\varepsilon = \frac{\sigma}{E_i}\left[1 + \left(\frac{a}{r+1}\right)\left(\frac{|\sigma|}{\sigma_y}\right)^r\right] \tag{35}$$

and the properties listed in Table 2. However, they showed negligible divergence from the bi-linear elasto-plastic analyses and are not presented herein.

The properties of the soil-springs (Table 3) were calculated according to the ALA–ASCE [3] guidelines, assuming that the pipeline top is buried under 1.30 m of medium-density sand with friction angle $\varphi = 36^\circ$ and unit weight $\gamma = 18\,\mathrm{kN/m^2}$. The fault movement was applied statically at the sliding part of the fault, as a permanent displacement of the free end of the corresponding soil-springs.

The results of the numerical analyses are presented in Fig. 10 in comparison with analytical predictions of the proposed methodology, as well as the analytical methodologies of Kennedy et al. [4] and Wang and Yeh [7]. The comparison is shown in terms of:

- the axial strain at the intersection of the pipeline with the fault trace,
- the maximum axial strain,
- the bending strain and
- the maximum total strain.

Three (3) different fault cases are examined, with intersection angles of $\beta = 30^\circ$, 45° and 60°. In each case, the analysis proceeded incrementally to a final fault displacement $\Delta f = 2D$, with D being the pipeline's external diameter. Note that bending strains corresponding to the Wang and Yeh [7] method were derived from Eq. (21), consistently with the assumption that pipeline segments AB and BC deform as circular arcs (Fig. 1).

The top row of Fig. 10 shows the comparison between analytical and numerical predictions of axial strain $\varepsilon_{a,fault}$ at the pipeline-fault trace intersection. The agreement appears fairly good, for all analytical methods. As the main assumption for computing $\varepsilon_{a,fault}$ is the compatibility between the geometrically required and the stress induced (available) elongation of the pipeline, the observed agreement is essentially considered as a solid verification of this assumption.

The second row of Fig. 10 refers to the overall maximum axial strain $\varepsilon_{a,max}$, which does not necessarily develop at the pipeline-fault trace intersection, as the existing analytical methods imply. In this case, a good overall agreement is observed only between numerical results and analytical predictions with the proposed methodology. The existing analytical methods approach the numerical solution at large displacements, after the yield strain of the pipeline steel has been exceeded, while they grossly under-predict $\varepsilon_{a,max}$ at smaller displacements. Note that observed differences are larger at intermediate displacement levels, of the order of $\Delta f \approx 1D$, which are commonly encountered in practice.

Focusing next on bending strains ε_b, a good overall agreement is observed again between the proposed analytical method and the numerical analyses. The Kennedy et al. [4] method proves accurate in the region of large displacements ($\Delta f/D > 1.5$), i.e. when the criteria for the applicability of the method are met, but seriously over-predicts ε_b for smaller fault displacements. The Wang and Yeh [7] method under-predicts ε_b for the entire range of fault displacements analyzed herein, mainly because it neglects the effect of axial tension on the pipeline bending stiffness.

The maximum longitudinal strains $\varepsilon_{max} = \varepsilon_{a,max} + \varepsilon_b$ are probably the best criterion for the evaluation of the proposed methodology, as they form the basis of pipeline design. From the last row of Fig. 10, it may be observed that the good overall performance of the proposed method, acknowledged in the previous comparisons, applies here as well. As expected, the Kennedy et al. [4] method over-predicts maximum strains for small fault displacements. This trend is reversed at intermediate levels of fault displacement, and the divergence is gradually reduced as displacements increase. Finally, the methodology of Wang and Yeh [7] provides accurate results only in the region of large displacements, where axial tension is the prevailing mode of deformation. For small and intermediate fault displacements ε_{max} is consistently under-estimated.

5. Conclusion

An improved analytical methodology has been developed for the stress analysis of buried steel pipelines crossing active strike-slip faults. It is based on firm assumptions adopted in the existing analytical methodologies of Kennedy et al. [4] and Wang and Yeh [7], but proceeds further:

- to analyze the curved part of the pipeline with the aid of elastic-beam theory, in order to locate the most unfavorable combination of axial and bending strains, and
- to consider the actual stress distribution on the pipeline cross-section, in order to account for the effect of curvature on axial strains and calculate the design maximum strain.

Comparison with the results of benchmark numerical analyses, performed over a wide range of fault displacements ($\Delta f/D = 0 \div 2$) and three different intersection angles ($\beta = 30^\circ$, 45° and 60°), showed a remarkable overall agreement, with minor deviations which did not exceed about 10%.

Acknowledging that there is no end to the refinements that can be applied to simplified analytical methodologies, it needs

to be stressed out that the above modifications considerably improve the accuracy of analytical predictions, especially for small and medium fault displacements, while they still permit a simple analytical solution algorithm to be developed. In fact, although more complicated than the most commonly used today method of Kennedy et al. [4], the computational algorithm of the proposed methodology remains relatively simple and stable, and can be easily programmed for quick application. For instance, such a computer code may be downloaded from http://users.civil.ntua.gr/gbouck/en/publications.htm.

Note that, in its present form, the proposed method applies to intersection angles $\beta \leqslant 90^\circ$ resulting in elongation of the pipeline. Furthermore, it does not account for the effects of local buckling and section deformation. Therefore, its application should not be extended beyond the strain limits explicitely defined by design codes in order to mitigate such phenomena.

Acknowledgements

This research is supported by the "EPEAEK II—Pythagoras" Grant, co-funded by the European Social Fund and the Hellenic Ministry of Education.

References

[1] EERI. The Izmit (Kocaeli), Turkey Earthquake of August 17, 1999. EERI Special Earthquake Report, 1999.

[2] Uzarski J, Arnold C. Chi-Chi, Taiwan, Earthquake of September 21, 1999, Reconnaissance Report. Earthquake Spectra, Professional J EERI 2001;17(Suppl. A).

[3] American Lifelines Alliance—ASCE. Guidelines for the Design of Buried Steel Pipe, July 2001 (with addenda through February 2005).

[4] Kennedy RP, Chow AW, Williamson RA. Fault movement effects on buried oil pipeline. Transport Eng J ASCE 1977;103:617–33.

[5] ASCE Technical Council on Lifeline Earthquake Engineering. Differential Ground Movement Effects on Buried Pipelines. Guidelines Seismic Des Oil Gas Pipeline Syst 1984:150–228.

[6] Newmark NM, Hall WJ. Pipeline design to resist large fault displacement. In: Proceedings of the US National Conference on Earthquake Engineering. Ann Arbor: University of Michigan; 1975. p. 416–25.

[7] Wang LRL, Yeh Y. A refined seismic analysis and design of buried pipeline for fault movement. Earthquake Eng Struct Dyn 1985;13:75–96.

[8] Calladine CR. Theory of shell structures. Cambridge: Cambridge University Press; 1983.

[9] CEN European Committee for Standardisation, Eurocode 8: Design of structures for earthquake resistance, Part 4: Silos, tanks and pipelines, Draft No 2, Ref. No. EN1998-4: 2003 (E), December 2003.

[10] Takada S, Hassani N, Fukuda K. A new proposal for simplified design of buried steel pipes crossing active faults. Earthquake Eng Struct Dyn 2001;30:1243–57.

[11] Hansen JB. The ultimate resistance of rigid piles against transversal forces. Bulletin 12. Copenhagen, Denmark: Danish Geotechnical Institute; 1961.

[12] Trautmann CH, O'Rourke TD. Behavior of pipe in dry sand under lateral and uplift loading. Geotechnical Engineering Report 83-6. Cornell University, Ithaca, New York, 1983.

[13] The MacNeal—Schwendler Corporation. MSC/NASTRAN for Windows: Reference Manual, 1994.